Evaluating the Timing and Structure of the 4.2 ka BP Event in the Indian Summer Monsoon Domain from an Annually-Resolved Speleothem Record from Northeast India

Gayatri Kathayat[1*], Hai Cheng[1, 2*], Ashish Sinha[3], Max Berkelhammer[4], Haiwei Zhang[1], Pengzhen Duan[1], Hanying Li[1], Xianglei Li[1], Youfeng Ning[1], Richard Lawrence Edwards[2]

[1] Institute of Global Environmental Change, Xi'an Jiaotong University, China
[2] Department of Earth Sciences, University of Minnesota, Minneapolis, USA
[3] Department of Earth Science, California State University Dominguez Hills, Carson, USA
[4] Department of Earth and Environmental Sciences, University of Illinois, Chicago, USA

Correspondence to: Gayatri Kathayat (kathayat@xjtu.edu.cn) & Hai Cheng (cheng021@xjtu.edu.cn).

Abstract

A large array of proxy records suggests that the '4.2 ka event' marks an ~ three hundred years long period (~3.9 to 4.2 ka BP) of major climate change across the globe. However, the climatic manifestation of this event, including its onset, duration, and termination, remains less clear in the Indian summer monsoon (ISM) domain. Here, we present new oxygen isotope ($\delta^{18}O$) data from a pair of speleothems (ML.1 and ML.2) from Mawmluh Cave, Meghalaya, India that provide a high-resolution record of ISM variability during a period (~3.78 and 4.44 ka BP) that fully encompasses the 4.2 ka event. The sub-annually to annually resolved ML.1 $\delta^{18}O$ record is constrained by 18 ^{230}Th dates with average dating error of ±13 years (2σ) and resolution of ~40 years, which allow us to characterize the ISM variability with an unprecedented detail. The inferred pattern of ISM variability during the period contemporaneous with the '4.2 ka event' shares broad similarities as well as key differences with the previous reconstructions of ISM from the Mawmluh Cave and other proxy records from the region. Our data suggest that the ISM intensity, in the context of the length of our record, abruptly decreased at ~4.0 ka BP (~± 13 years), marking the onset of a multicentennial period of relatively reduced ISM, which was punctuated by at least two multidecadal droughts between the ~3.9 and 4.0 ka BP. The latter stands out in contrast with some previous proxy reconstructions of the ISM, in which the '4.2 ka event' have been depicted as a singular multi-centennial drought.

1. Introduction

The time interval between 4.2 and 3.9 ka BP (thousand years before present, where present =1950 AD) constitutes an important period from both climatological and archeological perspectives (e.g., Weiss et al., 1993; Cullen et al., 2000; Staubwasser et al., 2003; Berkelhammer et al., 2012; Weiss, 2016). A global suite of proxy records shows widespread climate anomalies during the time (commonly referred as the '4.2 ka event') (e.g., Cullen et al., 2000; Staubwasser et al., 2003; Arz et al., 2006; Drysdale et al., 2006; Menounos et al., 2008; Liu and Feng, 2012; Berkelhammer et al., 2012; Dixit et al., 2014, 2018; Cheng et al. 2015; Nakamura et al., 2016; Railsback et al., 2018). Additionally, a number of archeological studies also suggest that the '4.2 ka event' was associated with a series of cultural and societal changes in the Mediterranean, Middle East, Africa, South and East Asia (e.g., Weiss et al.,1993; Enzel et al., 1999; Cullen et al., 2000; Staubwasser et al., 2003; Marshall et. al., 2011; Liu and Feng, 2012; Dixit et al., 2014; Weiss, 2016). For example, the '4.2 ka event' has been proposed to have contributed to collapses of the early Bronze age civilizations, including the Longshan Culture in China (Chang, 1999; Liu and Feng, 2012), Egyptian Old Kingdom by the Nile River (Stanley et al., 2003), and the Akkadian Empire in Mesopotamia (Weiss et al.,1993; Cullen et al., 2000). In South Asia, the 4.2 ka event has been linked to a weakening of the Indian summer monsoon (ISM) and the ensuing deurbanization of the Indus Valley Civilization (Staubwasser et al., 2003; Madella and Fuller, 2006; Dixit et al., 2014; Giosan et al., 2012; Berkelhammer et al., 2012; Kathayat et al., 2017; Dixit et al., 2018).

A number of proxy records from the Indian subcontinent suggest that a major weakening of the ISM occurred around the '4.2 ka event' (Staubwasser et al., 2003; Berkelhammer et al., 2012; Dixit et al., 2014; Nakamura et al., 2016; Kathayat et al., 2017) (Figs. 1 and 2). The 4.2 ka event has been generally described as an approximately a two to three-centuries-long interval of drought (e.g., Berkelhammer et al., 2012; Dixit et al., 2014; Nakamura et al., 2016), which was superimposed on a longer-term insolation-induced weakening of the ISM during the Holocene (e.g., Kathayat et al., 2017). The timing, structure and magnitude of the 4.2 ka event in the ISM regime however, remain unclear because most proxy records from the region have low temporal precision and insufficient resolution to precisely characterize the event (e.g., Staubwasser and Weiss, 2006; Prasad and Enzel, 2006; Nakamura et al., 2016; Dixit et al., 2018). In addition, the 4.2 ka event is notably absent in a recent high-resolution speleothem

oxygen isotope (δ^{18}O) record from Sahiya Cave in northern India (Kathayat et al., 2017) that

70　　exhibits a long-term drying trend from ~4.2 to 3.5 ka BP.

A high-resolution (~6 years) δ^{18}O record (KM-A) from Mawmluh Cave, located in the state of Meghalaya in Northeast India has previously provided evidence of the '4.2 ka event' from the ISM domain (Berkelhammer et al. 2012). The KM-A record was recently used to

75　　formally ratified the post-4.2 ka BP time as the Meghalayan Age (Walker et al., 2018). However, the timing and duration of the 4.2 ka event in the KM-A record is constrained by only three ^{230}Th dates (5048 ±32, 4112 ±30 and 3654 ±20 ka BP) and additionally, the youngest date defining the termination of the event and/or the δ^{18}O values from the top ~30 mm of the KM-A sample that help define the event may have been potentially affected by diagenetic

80　　changes. In this study, we present new high-resolution δ^{18}O data from two stalagmites (ML.1 and ML.2) from the same cave (Figs. 1 and 3, Table. 1). The ML.1 and ML.2 δ^{18}O records span from 4.44 to 3.78 ka BP and 4.53 to 3.70 ka BP, respectively, encompassing the 4.2 ka event completely. Our new records are sub-annually to annually (ML.1) and sub-decadally resolved (ML.2) and have unprecedented chronologic constraints, which allow us to

85　　characterize the nature of ISM variability during the 4.2 ka event more precisely than previously possible.

2 Samples and Methods
2.1 Cave location and climatology

90　　Mawmluh Cave (25°15′32″N, 91°42′45″E, 1290 m asl) is located near the town of Sohra (Cherrapunji) at the southern fringe of the Meghalayan Plateau in Northeast India (Fig. 1). The mean annual rainfall is ~11,000 mm in the region, 70% of which falls during the peak ISM months (June-September) (Murata et al., 2007). The rainfall at the cave site during the ISM period is mainly produced by convective systems and low-level air parcels originated from the

95　　Bay of Bengal, which propagates further northward and penetrate farther into the Tibetan Plateau (Sengupta and Sarkar, 2006; Breitenbach et al., 2010). The non–monsoonal component of rainfall is trivial and consists of the westerly related moisture as well as recycled local moisture (Breitenbach et al., 2010, 2015; Berkelhammer et al., 2012). The cave is overlain by 30–100 m thick and heavily karstified host rock (limestone, sandstone, and a 40–100 cm thick

100　　coal layer) (Breitenbach et al., 2010). The soil layer above the cave is rather thin (5–15 cm)

and covered mainly by grasses and bushes. Cave monitoring data (Breitenbach et al., 2010) indicate that the relative humidity inside the cave is more than 95% even during the dry season (November to April). Temperature variations in the cave are small (18.0–18.5°C) and close to the mean annual temperature of the area (Breitenbach et al., 2010, 2015). A 3-year cave monitoring results suggest that cave drip-water $\delta^{18}O$ signals lag corresponding local rainfall by less than 1 month, and thus preserve seasonal signals of ISM rainfall (Breitenbach et al., 2010). Previous studies have indicated that variations in the $\delta^{18}O$ of speleothem calcite from Mawmluh Cave reflect changes in the amount-weighted $\delta^{18}O$ of precipitation ($\delta^{18}O_p$) values (Breitenbach et al., 2010 and 2015; Berkelhammer et al., 2012; Myers et al., 2015). The ML.1 and ML.2 samples from Mawmluh Cave were collected in November 2015 at ~4–5 m above the cave floor and ~700 m from the cave entrance. Diameters of ML.1 and ML.2 are ~170 and 165 mm, and lengths ~315 and ~311 mm, respectively. Both stalagmite samples were cut along their growth axes using a thin diamond blade. There are no visible changes in the texture or hiatuses in the above sample intervals that we used for this study (Fig. 3).

2.2 ^{230}Th dating

We obtained 18 and 5 ^{230}Th dates for samples ML. 1 and ML. 2, respectively. Sub-samples for ^{230}Th dating (~30 mg) were drilled from ML.1 and ML.2 by using a 0.5 mm carbide dental drill. The ^{230}Th dating was performed at the Xi'an Jiaotong University, China using Thermo-Finnigan Neptune-*plus* multi-collector inductively coupled plasma mass spectrometers (MC-ICP-MS). The method is described in Cheng et al. (2000, 2013). We used standard chemistry procedures (Edwards et al., 1987) to separate uranium and thorium. A triple-spike (^{229}Th–^{233}U–^{236}U) isotope dilution method was used to correct instrumental fractionation and to determine U/Th isotopic ratios and concentrations (Cheng et al., 2000, 2013). U and Th isotopes were measured on a MasCom multiplier behind the retarding potential quadrupole in the peak-jumping mode using the standard procedures described in Cheng et al. (2000). Uncertainties in U/Th isotopic measurements were calculated offline at 2σ level, including corrections for blanks, multiplier dark noise, abundance sensitivity, and contents of the same nuclides in spike solution. The U decay constants are reported in Cheng et al. (2013). Corrected ^{230}Th ages assume the initial ^{230}Th/^{232}Th atomic ratio of $4.4 \pm 2.2 \times 10^{-6}$, the values for material at secular equilibrium with the bulk earth ^{232}Th/^{238}U value of 3.8. The corrections are small because the uranium concentrations of the samples are high (~6 ppm) and detrital ^{232}Th components are low (average <170 ppt) in (Table 1 and Supplementary Table 1).

2.3 Age models

135

The ML.1 age models and associated age uncertainties were constructed using COPRA (Constructing Proxy Records from Age model) (Breitenbach et al., 2012), Bchron (Haslett et al., 2008) and ISCAM (Fohlmeister, 2012) age modeling schemes (Fig. 4). All three modeling schemes yielded nearly identical results and the conclusions of this study are then not sensitive

140   to the choice of different age models (Fig. 4). The ML.2 age model and associated uncertainties were constructed by only using the COPRA age modeling scheme (Breitenbach et al., 2012) (Fig. 4).

2.4 Stable isotope analysis

145

The ML.1 and ML.2 $\delta^{18}O$ records are established by ~970 and ~238 stable isotope measurements, respectively (Figs. 5, 6 and Supplementary Table 2). Subsamples for stable isotope measurements were obtained from ML.1 and ML.2 between depths 125–250 mm and 182–255 mm (depth from the top), respectively. Accordingly, we report our data with zero depths set at 125 mm and 182 mm from the top of stalagmites ML.1 and ML.2, respectively

150   (Fig. 3). We used New Wave Micromill, a digitally controlled tri-axial micromill equipment, to obtain the subsamples. The sample growth rates were determined by sample age models, which in turn, were used to determine the sub-sampling increments (typically between 50 and 100 μm) for attaining similar temporal resolutions throughout the sample (typically ~1 year for the ML.1 $\delta^{18}O$ record). The $\delta^{18}O$ and $\delta^{13}C$ were measured using Finnigan MAT-253 mass

155   spectrometer coupled with an on-line carbonate preparation system (Kiel-IV) in the Isotope Laboratory, Xi'an Jiaotong University. Results are reported in per mil (‰) relative to the Vienna PeeDee Belemnite (VPDB) standard. Duplicate measurements of standards NBS19 and TTB1 show a long-term reproducibility of ~0.1‰ (1σ) or better (Figs. 5, 6 and Supplementary Table 2)

160 ## 2.5 Replication and isotopic equilibrium

Excellent replication between the ML.1 and ML.2 $\delta^{18}O$ profiles (Fig. 5) suggest that the precipitation of speleothem calcite in Mawmluh Cave essentially occurred at or near isotopic equilibrium conditions and the speleothem $\delta^{18}O$ records reflects primarily the meteoric precipitation $\delta^{18}O$ variations (Dorale et al., 1998; Wang et al., 2001). A high degree of

replication has been argued as a definitive test of isotopic equilibrium. This is because if the records replicate, the effect of additional kinetic/vadose-zone processes on the calcite $\delta^{18}O$ must have been either absent or the exactly same for spatially separated stalagmites. Principally, each speleothem-drip-water pair can have distinctive combination of flow-path, CO_2 content, residence time, solute concentrations, and prior calcite precipitation (PCP) history in the soil zone and epikarst above cave. Thus, the replication of different speleothem records suggests that such additional processes are not crucial. We assessed the degree of replication between ML.1 and ML.2 $\delta^{18}O$ records by using the ISCAM (Intra-Site Correlation Age Modeling) algorithm (Fohlmeister, 2012). The ISCAM finds the best correlation between proxy records within the combined age uncertainties of two records by using a Monte Carlo approach. Significant levels were calculated against a red-noise background from 1,000 pairs of artificially simulated first-order autoregressive time series (AR1). The ML.1 and ML.2 $\delta^{18}O$ time series on ISCAM derived age models display a statistically significant correlation (r = 0.58 at 95% confidence level) over their contemporary growth period between ~4.4 and 3.8 ka BP.

3 Results

3.1 Results

The average ^{230}Th dating uncertainties of the ML.1 and ML.2 records are ±13 and ±16 years, respectively (Fig. 3, Table 1 and Supplementary Table 1). Temporal resolutions of the ML.1 $\delta^{18}O$ record range from ~0.1 to ~3 years with an average resolution of ~1 year. All dates are in stratigraphic order within dating uncertainties. Of note, 9 ML.1 ^{230}Th dates were obtained between 27 and 88 mm depths (i.e., about one date every 7 mm), covering the interval from 4.2 to 3.9 ka BP, the typical time range of the 4.2 ka event. The ML.1 and ML.2 $\delta^{18}O$ values range between -6.6 and -4.8 ‰ with the mean values of -5.80 and -5.43‰, respectively (Fig. 5). The average temporal resolution of the ML.2 record is ~5 years (Fig. 5). The $\delta^{13}C$ values in ML.1 and ML.2 ranges between -2.8‰ and 1.0‰ with the mean values of -1.0‰ and -0.8‰ respectively (Fig. 6).

4 Discussion and Conclusions

4.1 Proxy interpretations

195   The temporal variability in ISM $\delta^{18}O_p$ and consequently, speleothem $\delta^{18}O$ in the study area, has been well studied previously and attributed mainly to changes in spatially-integrated upstream rainfall of cave sites (e.g., Sinha et al., 2011; Breitenbach et al., 2010, 2015; Berkelhammer et al., 2012; Kathayat et al., 2016; Cheng et al., 2016). A number of model simulations with isotope-enabled general circulation models (GCMs) also suggest a significant

200   inverse relationship between upstream ISM rainfall amount and the $\delta^{18}O_p$ variations over the Indian subcontinent (e.g., Vuille et al., 2005; Pausata et al., 2011; Berkelhammer et al., 2012; Sinha et al., 2015; Midhun and Ramesh, 2016). Following these reasonings, we interpret the low and high $\delta^{18}O$ values in our records to reflect strong and weak ISM, respectively (e.g., Dayem et al., 2010; Sinha et al., 2011, 2015; Cheng et al., 2012; Berkelhammer et al., 2012;

205   Breitenbach et al., 2015; Myers et al., 2015; Kathayat et al., 2016; Kathayat et al., 2017). Climatic interpretation of speleothem $\delta^{13}C$ signal are however, more complex because the $\delta^{13}C$ variations can be driven by climatic changes as well as non-climate related local processes (Baker et al., 1997; Genty et al., 2003; Fairchild et al., 2009; Fohlmeister et al., 2011; Deininger et al., 2012; Scholz et al., 2012). A moderate to strong covariance between the ML.1 and ML.2

210     $\delta^{13}C$ and $\delta^{18}O$ profiles value ($r= 0.49$ and 0.66, respectively) suggest that both proxies reflect a common response to changes in local hydrology of the region, however we cannot rule out non-climate related factors in producing this observed relationship. Consequently, the interpretative framework used in this study is mostly based on the speleothem $\delta^{18}O$ variability.

215 **4.2 Comparisons between the KM-A and ML.1/ML.2 $\delta^{18}O$ records**

        The '4.2 ka event' in the KM-A record (Berkelhammer et al., 2012) manifests as a two-step change marked by an initial increase in the $\delta^{18}O$ values (~0.6‰) between ~4.31 and 4.30 ka BP followed by another abrupt increase between ~ 4.07 and 4.05 ka BP. The period between 4.05 and 3.87 ka BP in the KM-A profile is characterized by the most enriched $\delta^{18}O$ values

220   over the entire record (~1.5‰ higher than the background values before the event) (Fig. 7), delineating ~180 years of substantially weaker ISM. This multi-centennial period of enriched $\delta^{18}O$ values was terminated abruptly by a sharp return (<20 years) to depleted $\delta^{18}O$ values implying a resumption of stronger monsoon. The ML.1 and ML.2 $\delta^{18}O$ profiles during the contemporaneous period with the KM-A record however, exhibit no step-like increase around

225   ~4.3 ka BP and instead, an abrupt increase in the $\delta^{18}O$ values at ~4.01 ka BP, which are superimposed over a gradually increasing trends over the entire length of the records. The timings and magnitude of this abrupt increase in the $\delta^{18}O$ values in both ML.1 and ML.2

profiles are comparable to that observed in the KM-A profile (within the combined age uncertainties of both record) (Fig. 7). A key difference between the KM-A, ML.1 and ML.2 $\delta^{18}O$ profiles however, is the absence of a sharp decrease in the $\delta^{18}O$ values at ~3.87 ka BP in our records, which mark the termination of the 4.2 ka event in the KM-A record. One of possibilities of this apparent difference is due to the large uncertainties of the KM-A record. Another plausible source of the difference may stem from dissolution of speleothem calcite of the KM-A sample between 0 and 29 mm depths (corresponding to ~3.65 and 5.08 ka BP) (Fig. 7), which may have either altered the age of the top date of the KM-A (i.e., making it younger than its true age) or affected the $\delta^{18}O$ values of calcite during this period. However, without a comprehensive, petrographic examination of the KM-A sample, we are unable to assess the aforementioned reasons for such differences.

4.3 The ISM variability and possible climate forcing

The z-score transformed ML.1 $\delta^{18}O$ profile (Fig. 8) illustrates the ISM variability between ~3.8 and 4.6 ka BP. The z-score is calculated by using the equation of the form $z = (x - \mu)/\sigma$, where x represents the individual ML.1 $\delta^{18}O$ value and μ and σ are the mean and the standard deviation of the entire ML.1 $\delta^{18}O$ record. The interval marking the onset of 4.2 ka event in our record (~4.255 ka BP) is marked by a transition from a pluvial (inferred by the lower $\delta^{18}O$ values) to variable ISM (dry/wet) conditions, with the latter superimposed by a few short-term (< decade) droughts (Fig. 8). Subsequently, the period between 4.07 and ~4.01 ka BP is marked by persistently lower $\delta^{18}O$ values implying stronger ISM (Fig. 8). The latter was terminated by a rapid increase in the $\delta^{18}O$ values (~1.0‰, Fig. 5) suggesting an abrupt weakening of the ISM at ~4.01 ka BP that occurred within a period of ~10 years. Notably, as discussed above, the ML.1 and ML.2 $\delta^{18}O$ profiles show gradual increasing trends over the entire length of the record, which was punctuated by two multidecadal weak monsoon events centered at ~3.970 (~20 years) and ~3.915 (~25 years) ka BP, respectively (Fig. 8). These aspects of our ISM reconstruction differ from previous proxy records from the ISM domain, which typically portray the 4.2 ka event as a multi-century drought (e.g., Berkelhammer et al., 2012; Dixit et al., 2014). Our new data however, demonstrate that prominent decadal to multi-decadal variability together with intermittent occurrence of multidecadal periods of low rainfall was the dominant mode of ISM variability during the period coeval with the 4.2 ka event (Figs. 5 and 8). These observations are consistent with previous reconstructions of ISM variability from high-resolution proxy records from the Indian subcontinent over the last two millennia

(e.g., Sinha et al., 2011 and 2015; Kathayat et al., 2017) as well as during the instrumental period (e.g., Krishnamurthy et al., 2000; Goswami et. al., 2006a). Periodic perturbations in coupled modes of ocean-atmosphere variability, such as the El Niño Southern Oscillation (ENSO), and/or dynamical processes intrinsic to the monsoon system such as quasi-periodic episodes of intense ("Active") and reduced ("Break") monsoon rainfall, are key processes that are known to produce multidecadal periods of droughts over large parts of Asia. For instance, Sinha et al. (2011) suggest that ISM circulation can "lock" into decadal to multidecadal long periods of "break-dominated" mode of ISM circulation that promote enhanced convection over the eastern equatorial Indian Ocean, which in turn, suppresses convection and rainfall over the continental monsoon regions. Additionally, the source of multidecadal droughts may also stem from switch-on of the modern ENSO regime around the 4.2 ka event, which would presumably also weaken the ISM (e.g., Donders et al., 2008; Conroy et al., 2008).

In conclusion, our new record from the Mawmluh Cave in Meghalaya, India provides a high-resolution history of ISM during a period contemporaneous with the 4.2 ka event. While our record shares broad similarities with a previous lower-resolution (~6 years) reconstruction of ISM from the same cave (Berkelhammer et al., 2012), key differences between the two records are also evident, which are likely due to the more refined age controls (~9 ^{230}Th dates spanning the 4.2 ka event interval and higher (annual) temporal resolution of our record. Our reconstruction suggests that the ISM exhibited prominent decadal to multicentennial variability, including sporadic but prominent multidecadal periods of reduced ISM rainfall (droughts), during the period spanning the 4.2 ka event. These aspects of our reconstruction are qualitatively similar to ISM variability during the late and middle Holocene as inferred from the previous speleothem-based reconstructions of ISM from the Indian subcontinent (e.g., Kathayat et al., 2017).

5 Author Contributions

G.K. and H.C. designed the research and experiments. GK wrote the first draft of the manuscript. H.C. A.S. and M.B. revised the manuscript. G.K., H.C. and L.X.L. did the fieldwork and collected the samples. G.K., H.C., H.W.Z., and R.L.E. conducted the ^{230}Th dating. G.K., P.Z.D. and L.H.Y conducted the oxygen isotope measurements. All authors discussed the results and provided inputs on the manuscript.

6 Competing interests

The authors declare no competing financial interests.

8 Data and materials availability

All data needed to evaluate the conclusions in the paper are presented in the paper. Additional data related to this paper may be requested from the authors. The data will be archived at the NOAA National Climate Data Center (https://www.ncdc.noaa.gov/data-access/paleoclimatology-data). Correspondence and requests for materials should be addressed to G.K. (kathayat@xjtu.edu.cn) and H.C. (cheng021@xjtu.edu.cn).

References:

Arz, H.W., Lamy, F., Pätzold, J.: A pronounced dry event recorded around 4.2 ka in brine sediments from the northern Red Sea. Quaternary Research 66, 432–441, 2006.

Baker, A., Ito, E., Smart, P. L. & McEwan, R. F.: Elevated and variable values of 13C in speleothems in a British cave system. Chem. Geol. 136, 263–270, 1997.

Berkelhammer, M., Sinha, A., Stott, L., Cheng, H., Pausata, F., Yoshimura, K.: An abrupt shift in the Indian monsoon 4000 years ago. Climates, landscapes, and civilizations, 75–88, 2012.

Breitenbach, S.F., Adkins, J.F., Meyer, H., Marwan, N., Kumar, K.K., Haug, G.H.: Strong influence of water vapor source dynamics on stable isotopes in precipitation observed in Southern Meghalaya, NE India. Earth and Planetary Science Letters 292, 212–220, 2010.

Breitenbach, S.F.M., Rehfeld, K., Goswami, B., Baldini, J.U.L., Ridley, H.E., Kennett, D.J., Prufer, K.M., Aquino, V.V., Asmerom, Y., Polyak, V.J., Cheng, H., Kurths, J., Marwan, N.: COnstructing Proxy Records from Age models (COPRA). Clim. Past 8, 1765–1779, 2012.

Breitenbach, S.F.M., Lechleitner, F.A., Meyer, H., Diengdoh, G., Mattey, D., Marwan, N.: Cave ventilation and rainfall signals in dripwater in a monsoonal setting – a monitoring study from NE India. Chemical Geology 402, 111–124, 2015.

Chang K.C.: China on the eve of the Historical Period. In: Loewe M and and Shaughnessy EL (eds) The Cambridge History of Ancient China – From the Origins of Civilization to 221 BC. New York: Cambridge University Press, pp. 37–73, (1999).

Cheng, H., Edwards, R., Hoff, J., Gallup, C., Richards, D., Asmerom, Y.: The half-lives of uranium-234 and thorium-230. Chemical Geology 169, 17–33, 2000.

340   Cheng, H., Zhang, P., Spötl, C., Edwards, R., Cai, Y., Zhang, D., Sang, W., Tan, M., An, Z.: The climatic cyclicity in semiarid-arid central Asia over the past 500,000 years. Geophysical Research Letters 39, 2012.

Cheng, H., Edwards, R.L., Shen, C.-C., Polyak, V.J., Asmerom, Y., Woodhead, J., Hellstrom, J., Wang, Y., Kong, X., Spötl, C.: Improvements in 230 Th dating, 230 Th and 234 U half-life values, and

345   U–Th isotopic measurements by multi-collector inductively coupled plasma mass spectrometry. Earth and Planetary Science Letters 371, 82–91, 2013.

Cheng, H., Sinha, A., Verheyden, S., Nader, F.H., Li, X.L., Zhang, P.Z., Yin, J.J., Yi, L., Peng, Y.B., Rao, Z.G., Ning, Y.F., Edwards, R.L.: The climate variability in northern Levant over the past 20,000 years. Geophysical Research Letters 42, 8641–8650, 2015.

350   Cheng, H., Edwards, R.L., Sinha, A., Spötl, C., Yi, L., Chen, S., Kelly, M., Kathayat, G., Wang, X., Li, X.: The Asian monsoon over the past 640,000 years and ice age terminations. Nature 534, 640-646, 2016.

Conroy, J. L., Overpeck, J. T., Cole, J. E., Shanahan, T. M., and Steinitz-Kannan, M.: Holocene changes in eastern tropical Pacific climate inferred from a Galápagos lake sediment record, Quaternary

355   Science Reviews, 27, 1166-1180, 2008.

Cullen, H.M., Hemming, S., Hemming, G., Brown, F., Guilderson, T., Sirocko, F.: Climate change and the collapse of the Akkadian empire: Evidence from the deep sea. Geology 28, 379–382, 2000.

Dayem, K. E., Molnar, P., Battisti, D. S., & Roe, G. H.: Lessons learned from oxygen isotopes in modern precipitation applied to interpretation of speleothem records of paleoclimate from eastern

360   Asia. Earth and Planetary Science Letters, 295(1), 219–230, 2010.

Deininger, M., Fohlmeister, J., Scholz, D. & Mangini, A.: Isotope disequilibrium effects: The influence of evaporation and ventilation effects on the carbon and oxygen isotope composition of speleothems - A model approach. Geochimica et Cosmochimica Acta 96, 57–79, 2012.

Dixit, Y., Hodell, D.A., Giesche, A., Tandon, S.K., Gázquez, F., Saini, H.S., Skinner, L.C., Mujtaba,

365   S.A., Pawar, V., Singh, R.N.: Intensified summer monsoon and the urbanization of Indus Civilization in northwest India. Scientific reports 8, 4225–, 2018.

Dixit, Y., Hodell, D.A., Petrie, C.A.: Abrupt weakening of the summer monsoon in northwest India~ 4100 yr ago. Geology 42, 339–342, 2014.

Donders, T. H., Wagner-Cremer, F., and Visscher, H.: Integration of proxy data and model scenarios

370   for the mid-Holocene onset of modern ENSO variability, Quaternary Science Reviews, 27, 571-579, 2008.

Dorale, Jeffrey A., Edwards, R. Lawrence., Ito, Emi., González, Luis A.: Climate and Vegetation History of the Midcontinent from 75 to 25 ka: A Speleothem Record from Crevice Cave, Missouri, USA. Science 282, 1871–1874, 1998.

375

Drysdale, R., Zanchetta, G., Hellstrom, J., Maas, R., Fallick, A., Pickett, M., Cartwright, I., Piccini, L.: Late Holocene drought responsible for the collapse of Old World civilizations is recorded in an Italian cave flowstone. Geology 34, 101–104, 2006.

Edwards, R.L., Chen, J., Wasserburg, G.: 238 U 234 U 230 Th 232 Th systematics and the precise measurement of time over the past 500,000 years. Earth and Planetary Science Letters 81, 175–192, 1987.

Enzel, Y., Ely, L.L., Mishra, S., Ramesh, R., Amit, R., Lazar, B., Rajaguru, S.N., Baker, V.R., Sandler, A.: High-resolution Holocene environmental changes in the Thar Desert, northwestern India. Science 284, 125–128, 1999.

Fairchild, I. J. & Treble, P. C.: Trace elements in speleothems as recorders of environmental change. Quat. Sci. Rev. 28, 449–468. 2009.

Fohlmeister, J., Scholz, D., Kromer, B. & Mangini, A.:Modelling carbon isotopes of carbonates in cave drip water. Geochimica et Cosmochimica Acta 75, 5219–5228, 2011.

Fohlmeister, J.: A statistical approach to construct composite climate records of dated archives. Quaternary Geochronology 14, 48–56, 2012.

Genty, D., Blamart, D., Ouahdi, R., Gilmour, M., Baker, J. Jouzel, J., Van-Exter S.: Precise dating of Dansgaard-Oeschger climate oscillations in western Europe from stalagmite data. Nature 421, 833–837, 2003.

Giosan, L., Clift, P.D., Macklin, M.G., Fuller, D.Q., Constantinescu, S., Durcan, J.A., Stevens, T., Duller, G.A., Tabrez, A.R., Gangal, K.: Fluvial landscapes of the Harappan civilization. Proceedings of the National Academy of Sciences 109, E1688-E1694, 2012.

Goswami, B.N., Wu, G., Yasunari, T.: The annual cycle, intraseasonal oscillations, and roadblock to seasonal predictability of the asian summer monsoon. J. Clim. 19, 5078e5098, 2006a.

Haslett, J., Parnell, A.: A simple monotone process with application to radiocarbon-dated depth chronologies. Journal of the Royal Statistical Society: Series C (Applied Statistics) 57, 399–418, 2008.

Kathayat, G., Cheng, H., Sinha, A., Spötl, C., Edwards, R.L., Zhang, H., Li, X., Yi, L., Ning, Y., Cai, Y., Lui, W.L., Breitenbach, S.F.M.: Indian monsoon variability on millennial-orbital timescales. Scientific Reports 6, 24374, 2016.

Kathayat, G., Cheng, H., Sinha, A., Yi, L., Li, X., Zhang, H., Li, H., Ning, Y., Edwards, R.L.: The Indian monsoon variability and civilization changes in the Indian subcontinent. Science advances 3, e1701296, 2017.

Krishnamurthy, V., Shukla, J.: Intraseasonal and interannual variability of rainfall over India. J. Clim. 13, 4366e4377, 2000.

Liu, F., Feng, Z.: A dramatic climatic transition at ~4000 cal. yr BP and its cultural responses in Chinese cultural domains. Holocene 22, 1181e1197, 2012.

Madella, M., Fuller, D.Q.: Palaeoecology and the Harappan Civilisation of South Asia: a reconsideration. Quaternary Science Reviews 25, 1283–1301, 2006.

Marshall, M.H., Lamb, H.F., Huws, D., Davies, S.J., Bates, R., Bloemendal, J., Boyle, J., Leng, M.J., Umer, M., Bryant, C.: Late Pleistocene and Holocene drought events at Lake Tana, the source of the Blue Nile. Global and Planetary Change 78, 147–161, 2011.

Menounos, B., Clague, J.J., Osborn, G., Luckman, B.H., Lakeman, T.R., Minkus, R.: Western Canadian glaciers advance in concert with climate change circa 4.2 ka. Geophysical Research Letters 35, 2008.

Midhun, M., & Ramesh, R.: Validation of $\delta^{18}O$ as a proxy for past monsoon rain by multi-GCM simulations. Climate dynamics, 46(5-6), 1371–1385, 2016.

Murata, F., Hayashi, T., Matsumoto, J., Asada, H.: Rainfall on the Meghalaya plateau in northeastern India—one of the rainiest places in the world. Natural Hazards 42, 391–399. 2007.

Myers, C.G., Oster, J.L., Sharp, W.D., Bennartz, R., Kelley, N.P., Covey, A.K., Breitenbach, S.F.: Northeast Indian stalagmite records Pacific decadal climate change: Implications for moisture transport and drought in India. Geophysical Research Letters 42, 4124–4132, 2015.

Nakamura, A., Yokoyama, Y., Maemoku, H., Yagi, H., Okamura, M., Matsuoka, H., Miyake, N., Osada, T., Adhikari, D.P., Dangol, V.: Weak monsoon event at 4.2 ka recorded in sediment from Lake Rara, Himalayas. Quaternary International 397, 349–359, 2016.

Pausata, F. S., Battisti, D. S., Nisancioglu, K. H., & Bitz, C. M.: Chinese stalagmite [delta] 18O controlled by changes in the Indian monsoon during a simulated Heinrich event. Nature Geoscience, 4(7), 474-480., 2011.

Prasad, S., Enzel, Y.: Holocene paleoclimates of India. Quaternary Research 66, 442–453, 2006.

Railsback, L.B., Liang, F., Brook, G., Voarintsoa, N.R.G., Sletten, H.R., Marais, E., Hardt, B., Cheng, H., Edwards, R.L.: The timing, two-pulsed nature, and variable climatic expression of the 4.2 ka event: A review and new high-resolution stalagmite data from Namibia. Quaternary Science Reviews 186, 78–90, 2018.

Sarkar, S., Prasad, S., Wilkes, h., Riedel, N., Stebich, M., Basavaiah, N., Sachse, D.: Monsoon source shifts during the drying mid-Holocene: Biomarker isotope based evidence from the core 'monsoon zone' (CMZ) of India. Quaternary Science Reviews 123, 144–157, 2015.

Sabin, T., Krishnan, R., Ghattas, J., Denvil, S., Dufresne, J.-L., Hourdin, F., Pascal, T.: High resolution simulation of the South Asian monsoon using a variable resolution global climate model. Climate dynamics 41, 173–194, 2013.

Scholz, D., Frisia, S., Borsato, A., Spötl, C., Fohlmeister, J., Mudelsee, M., Miorandi, R., Mangini, A.: Holocene climate variability in north-eastern Italy: potential influence of the NAO and solar activity recorded by speleothem data. Clim. Past 8, 1367–1383, 2012.

Sengupta, S., Sarkar, A.: Stable isotope evidence of dual (Arabian Sea and Bay of Bengal) vapour sources in monsoonal precipitation over north India. Earth and Planetary Science Letters 250, 511–521, 2006.

450 Sinha, A., Kathayat, G., Cheng, H., Breitenbach, S.F., Berkelhammer, M., Mudelsee, M., Biswas, J., Edwards, R.: Trends and oscillations in the Indian summer monsoon rainfall over the last two millennia. Nature communications 6, 2015.

Sinha, A., Berkelhammer, M., Stott, L., Mudelsee, M., Cheng, H., Biswas, J.: The leading mode of Indian Summer Monsoon precipitation variability during the last millennium. Geophysical
455 Research Letters 38, 2011.

Sinha, A., Stott, L., Berkelhammer, M., Cheng, H., Edwards, R. L., Buckeley, B., Aldenderfer, M., Mudelsee, M.: A global context for megadroughts in monsoon Asia during the past millennium. Quat. Sci. Rev. 30, 47–62, 2011.

Stanley, J.-D., Krom, M.D., Cliff, R.A., Woodward, J.C.: Nile flow failure at the end of the Old
460 Kingdom, Egypt: strontium isotopic and petrologic evidence. Geoarchaeology: Int. J. 18, 395e402, 2003.

Staubwasser, M., Sirocko, F., Grootes, P., Segl, M.: Climate change at the 4.2 ka BP termination of the Indus valley civilization and Holocene south Asian monsoon variability. Geophysical Research Letters 30, 2003.

465 Staubwasser, M. and Weiss, H.: Holocene Climate and Cultural Evolution in Late Prehistoric-Early Historic West Asia. Quaternary Research 66, 372–387, 2006.

Vuille, M., Werner, M., Bradley, R. S., & Keimig, F.: Stable isotopes in precipitation in the Asian monsoon region. Journal of Geophysical Research: Atmospheres, 110(D23), n/a-n/a. doi: 10.1029/2005JD006022, 2005.

470 Walker, M., Head, M. j., Berkelhammer, M., Björck, s., Cheng, h., Cwynar, L., Fisher, D., Gkinis, V., Long, A., Lowe, J., Newnham, R., Olander, R. S., Weiss, H.: Formal ratification of the subdivision of the Holocene Series/ Epoch (Quaternary System/Period): two new Global Boundary Stratotype Sections and Points (GSSPs) and three new stages/ subseries. IUGS, 1–11, 2018.

Wang, Y. J., Cheng, H., Edwards, R. L., An,Z.S., Wu, J.Y., Shen,C.C., Dorale, A.J.: A high- Resolution
475 Absolute-Dated Late Pleistocene Monsoon Record from Hulu Cave, China. Science 294, 2345–2348, 2001.

Weiss, H.: Global megadrought, societal collapse and resilience at 4.2-3.9 ka BP across the mediterranean and west asia. PAGES 24, 62–63, 2016.

Weiss, H., Courty, M.-A., Wetterstrom, W., Guichard, F., Senior, L., Meadow, R., Curnow, A.: The
480 genesis and collapse of third millennium north Mesopotamian civilization. Science 261, 995–1004, 1993.
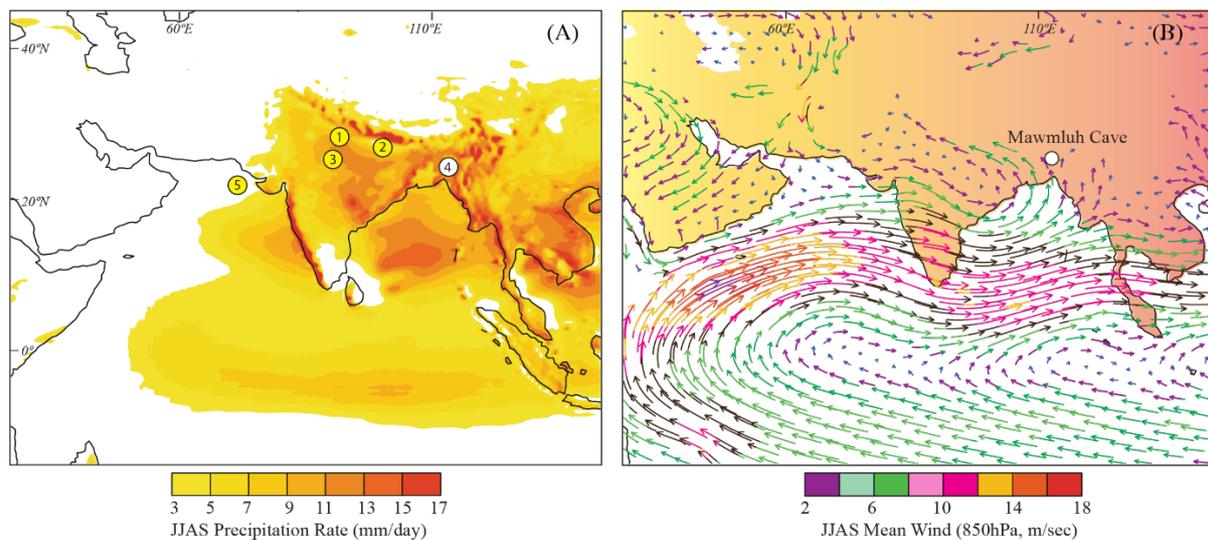
Figures


Figure 1. Location map and spatial structure of mean JJAS precipitation and low-level winds. (A) June-July-August-September (JJAS) precipitation from the Tropical Rainfall Measuring Mission (TRMM). The locations of Mawmluh Cave (white circle) and other proxy records mentioned in the text (yellow circles and numbers). The numbering scheme is as follows: 1, Sahiya cave (Kathayat et al., 2017); 2, Lake Rara (Nakamura et al., 2016); 3, Kotla Dhar (Dixit et al., 2014); 4, Mawmluh Cave (Berkelhammer et al., 2012); and 5, Indus Delta (Staubwasser et al., 2003). **(B)** 850 hPa-level monsoon vector from zoomed Laboratoire de Meteorologie Dynamique (LMDZ) general circulation model with telescoping zooming (figure adapted and modified from Sabin et al., 2013). The zoom version shows a well-defined cyclonic circulation with westerlies on the southern flanks and easterly winds on the northern flanks of the Monsoon Trough. The Mawmluh Cave is ideally located to record upstream variations in the overall strength of the ISM (see text).
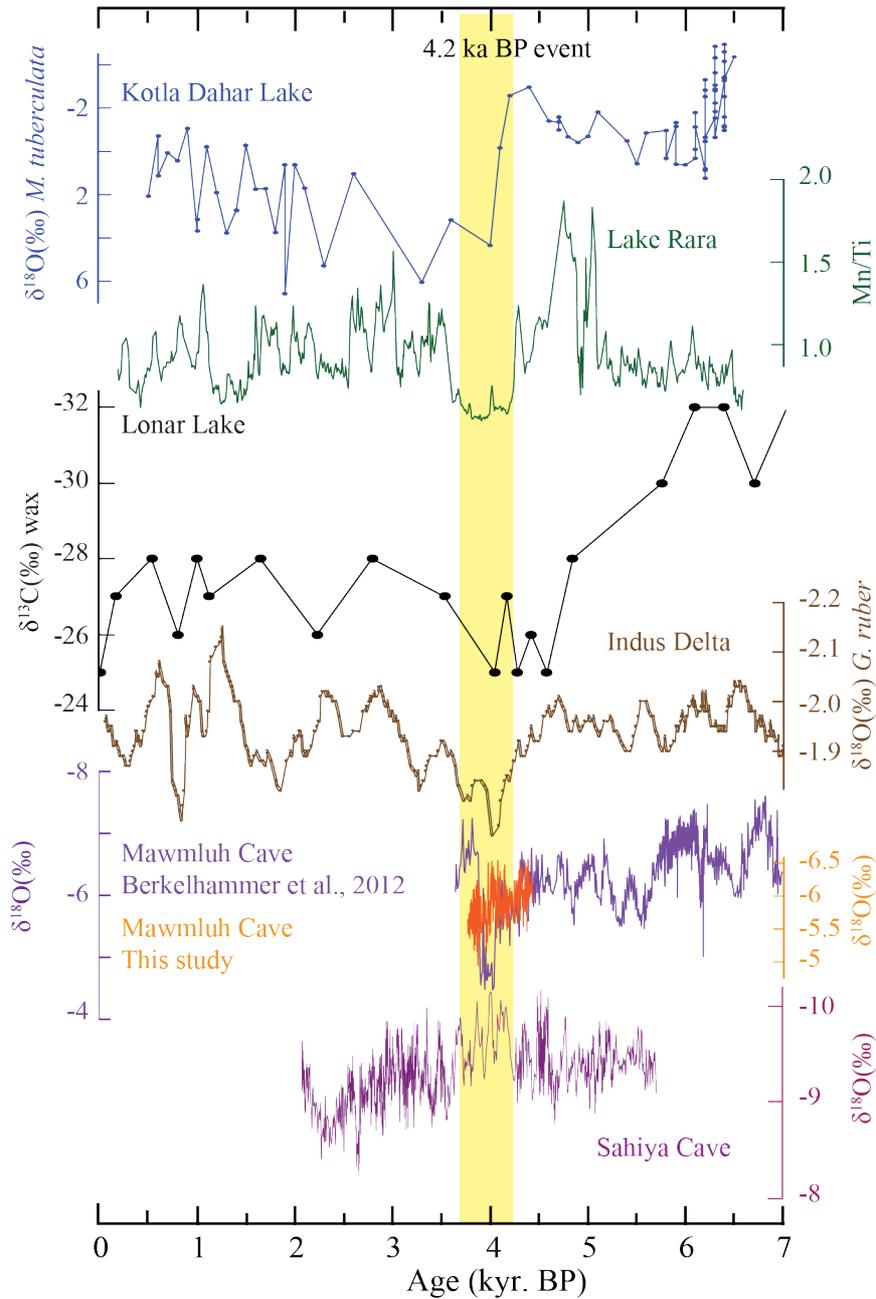
Figure 2. Proxy records from the Indian subcontinent. The select proxy records from the Indian monsoon domain from the top are Kotla Dhar (Dixit et al., 2014), Lake Rara (Nakamura et al., 2016), Lonar Lake (Sarkar et al., 2015), Indus Delta (Staubwasser et al., 2003), Mawmluh Cave (Berkelhammer et al., 2012, purple) and this study (orange), Sahiya Cave (Kathayat et al., 2017). The yellow bar delineates the commonly accepted temporal duration of the 4.2 ka BP event (e.g., Weiss et al., 2016).
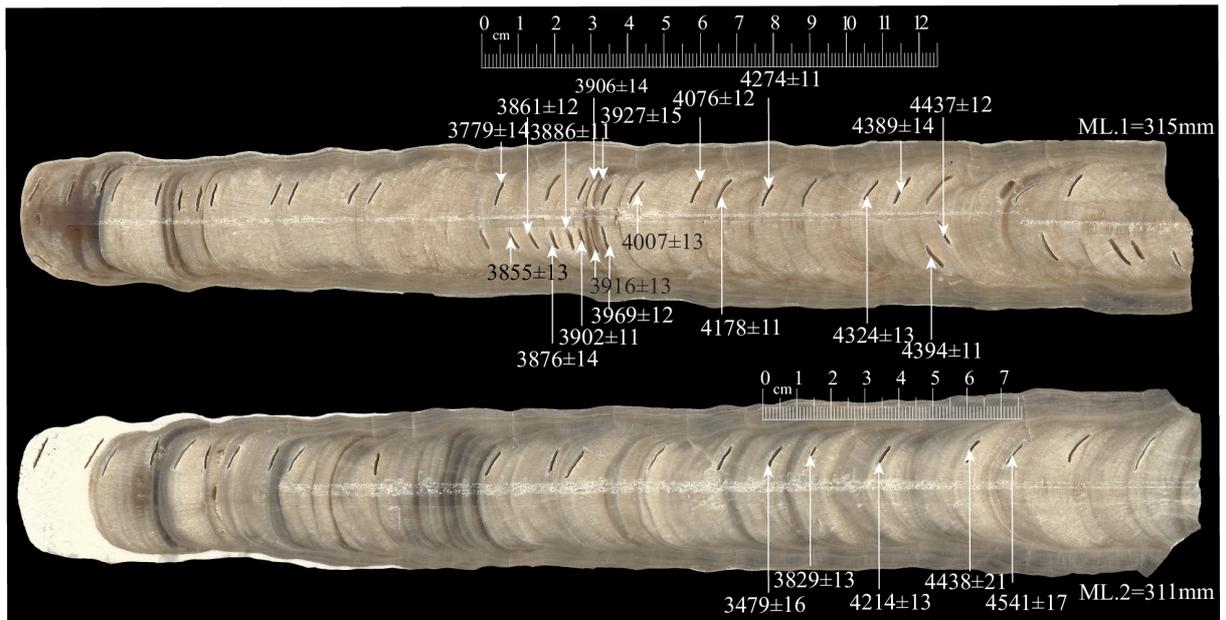
Figure 3. Samples photograph: The total length of ML.1 and ML.2 samples is 315 and 311mm respectively. The arrows indicate the dating sub-sampling location and the [230]Th dates with the 2σ analytical error (also see, Table 1 and Supplementary Table 1). The cm scale indicates the location of isotopic measurements, enclosing the interval of interest within both the samples.
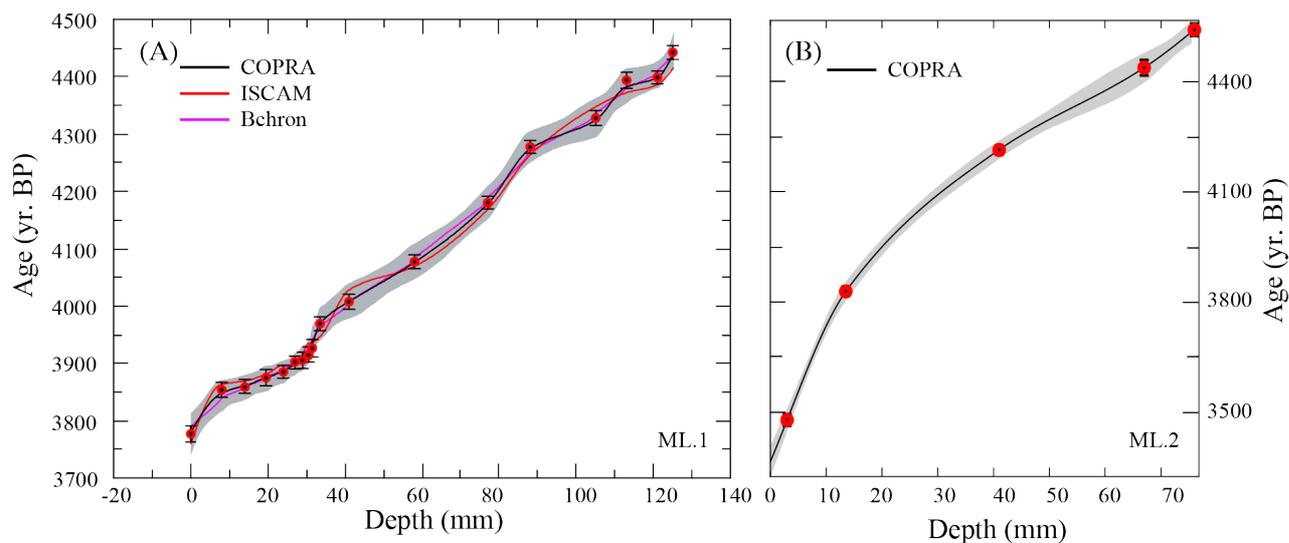
Figure 4. Age Models of ML.1 and ML.2 records. We adopted COPRA and generated 2000 realizations of age models to account for the dating uncertainties (2.5 and 97.5% quantile) confidence limits. **(A)** ML-1 age models and modeled age uncertainties using 3 different age-modeling algorithms, COPRA (black) (Breitenbach et al., 2012), Bchron (purple) (Haslett et al., 2008) and ISCAM (red) (Fohlmeister, 2012). The gray band depicts the 95% confidence interval using COPRA. Error bars on ^{230}Th dates represent a 2σ analytical error. **(B)** ML.2 age model and modeled age uncertainties using COPRA.
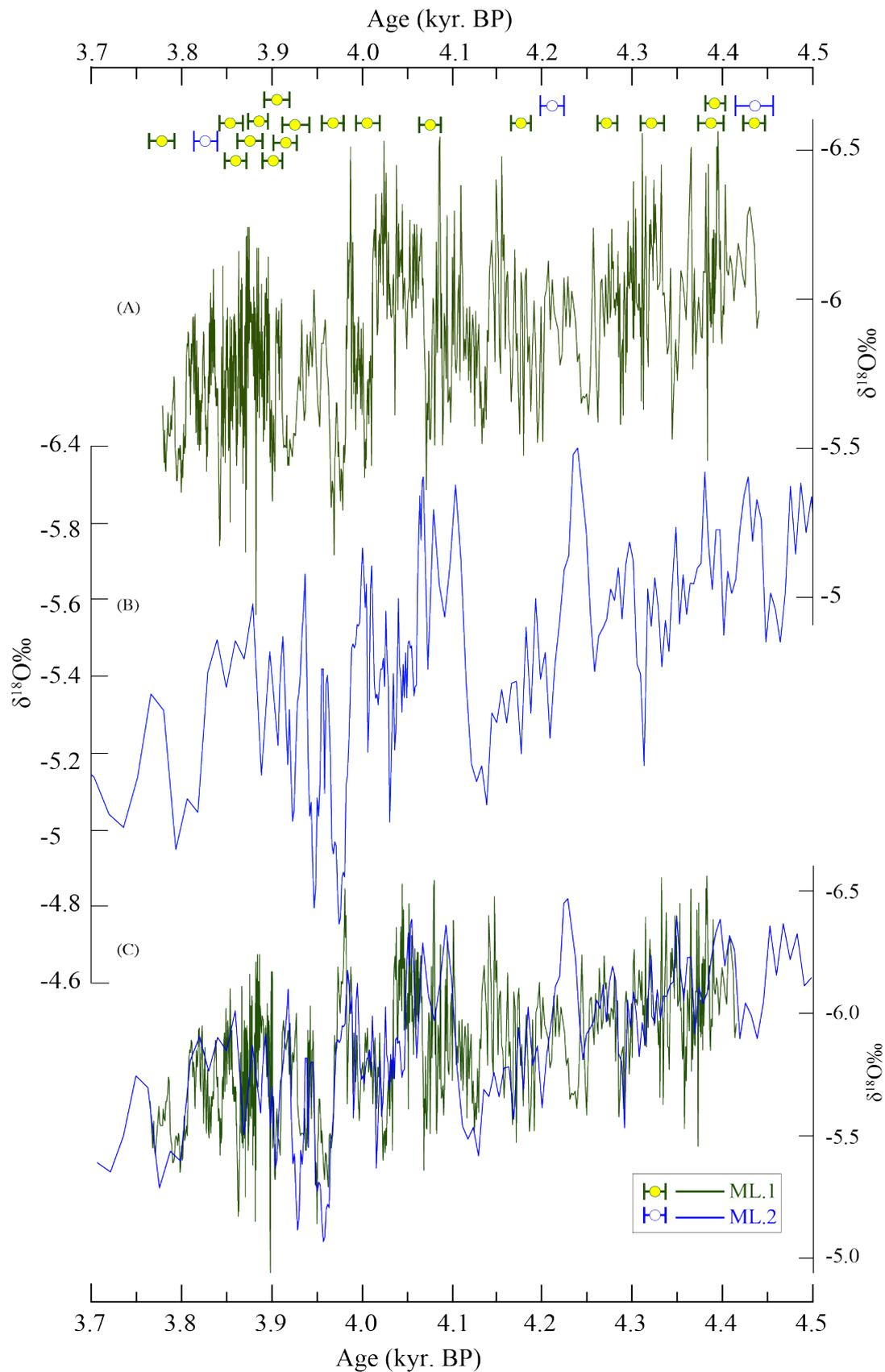
Figure 5. Comparison between ML.1 and ML.2 δ¹⁸O profiles over the period of overlap.
The ML.1 (A) and ML.2 (B) profiles are on their independent age models. The circles with
horizontal error bars depict [230]Th dates and errors (2σ) (also see Table 1 and Supplementary

Tables 1 and 2). (**C**) Comparison between the ML.1 and ML.2 δ^{18}O profiles based on ISCAM algorithm (Fohlmeister, 2012).

545
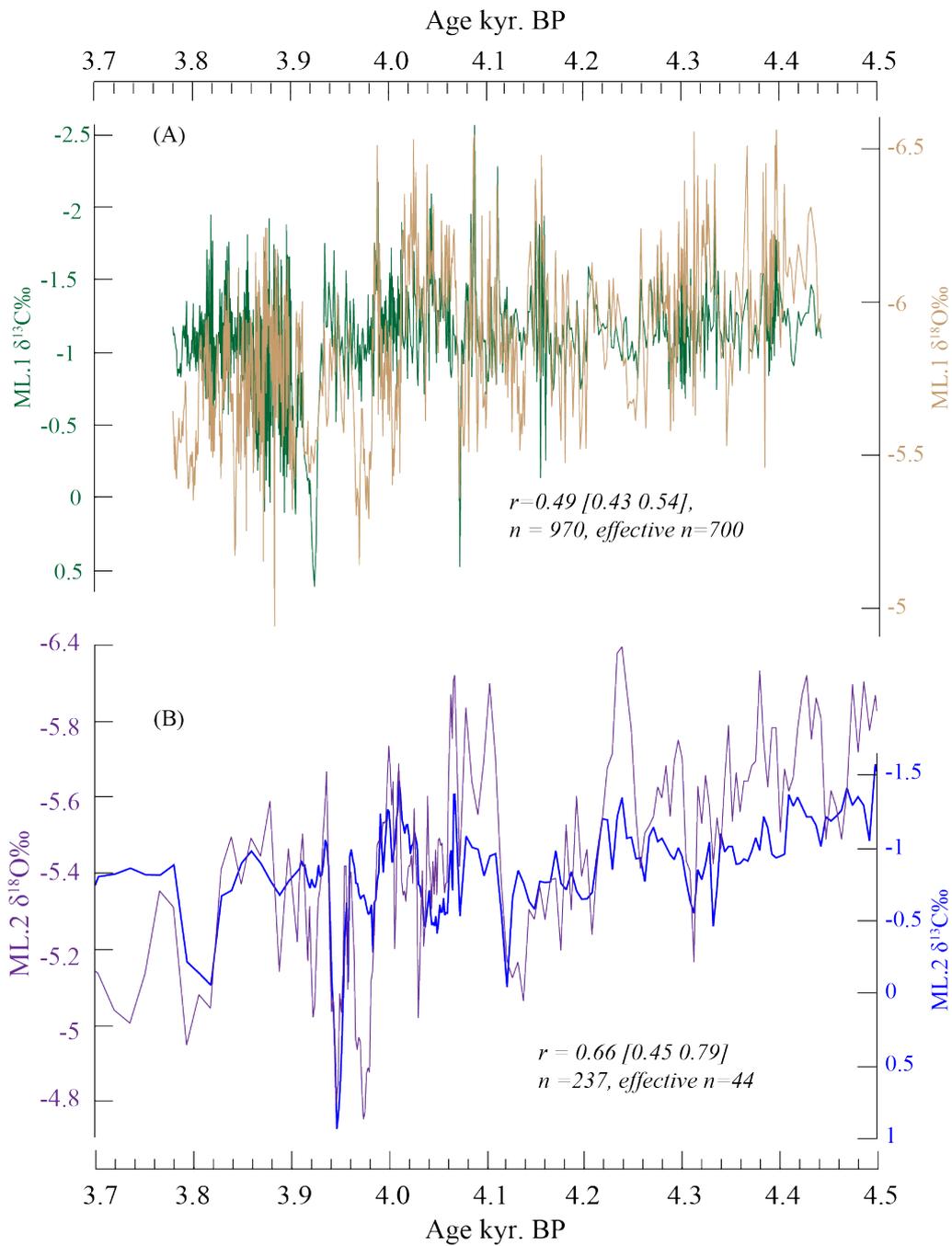
Figure 6. The **δ^{18}O and δ^{13}C profiles of ML.1 and ML.2. (A)** The ML.1 δ^{18}O (orange) and δ^{13}C (green). **(B)** The ML.2 δ^{18}O (purple) and δ^{13}C (blue) on their independent age models. The Pearson correlation (r) and its 95% confidence interval together with actual and effective

550 sample size (after considering autocorrelation in each profile) are shown on the figure.
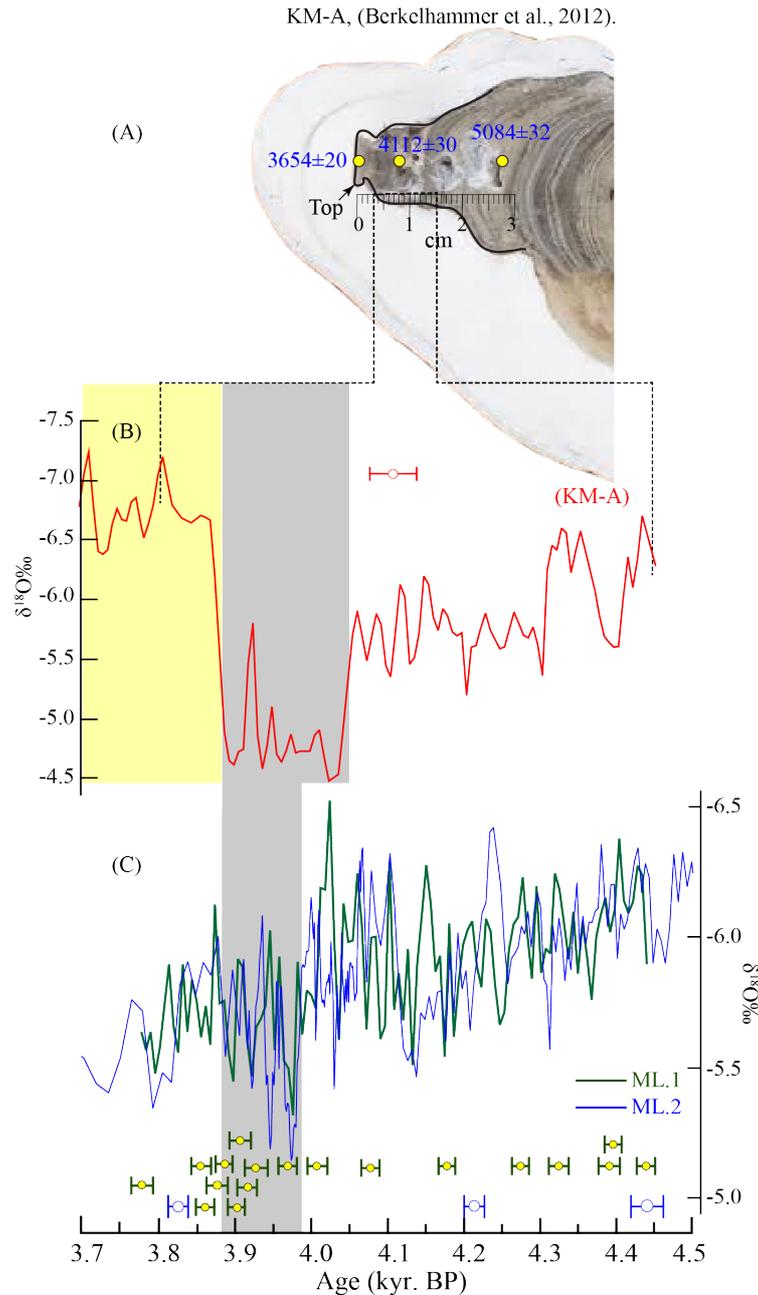
Figure 7. Comparison between the KM-A, ML.1, and ML2 $\delta^{18}O$ **profiles: (A) An image of** KM-A stalagmite (Berkelhammer et al., 2012). The yellow dots indicate three [230]Th dates. The black curve marks the potential dissolution surface. The white aragonite layer above the dissolution surface was deposited after the 1950s with the advent of limestone mining above the Mawmluh Cave (Breitenbach et al., 2010). **(B)** The dotted lines delineate the portion of KM-A $\delta^{18}O$ record (red; ~4.4 ka to 3.654 ka BP) (Berkelhammer et al., 2012) discussed in the text. **(C)** The ML.2 $\delta^{18}O$ profile (blue) (this study) is overlaid by 6-years interpolated ML.1 $\delta^{18}O$ profile (green) (this study, also see, Supplementary Table 2). The horizontal error bars (red, green and blue) on the [230]Th dates represent a 2σ analytical error. The vertical grey bar indicates the inferred duration of weakest (driest phase) of ISM as indicated by the KM-A and ML $\delta^{18}O$ records. The yellow bar indicates the interval of anomalously depleted $\delta^{18}O$ values in KM-A record.
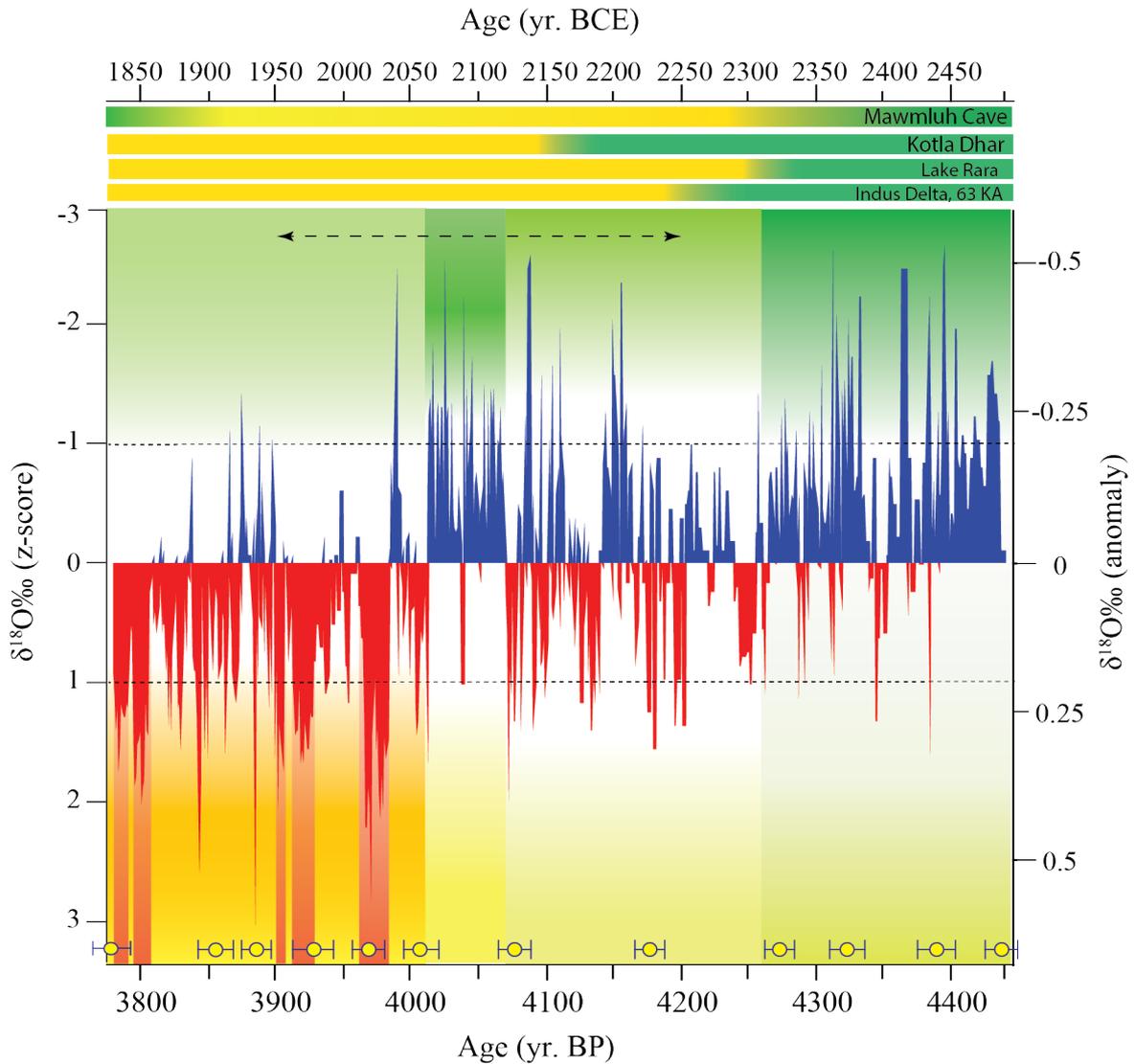
Figure 8. The inferred pattern of ISM variability during the 4.2 ka BP Event: The ML.1 $\delta^{18}O$ record is shown here as z-score (left y-axis) and anomalies (right y-axis) The horizontal dashed lines indicate one-standard deviation and the vertical color saturated shaded bars denote periods of inferred drier (yellow) pluvial (green) and variable conditions. The vertical red bars delineate the periods of multidecadal droughts (z-score > 1). The horizonal dashed double arrows mark the commonly accepted duration of the 4.2 ka event (see text) and the horizontal shaded bars indicate broad hydroclimate patterns inferred from other regional proxy records as mentioned in the text (also see Figs. 1 and 2). The circles with 2σ error bars show a subset of ^{230}Th dates (see Table 1 and Supplementary Table 1 for a complete listing of ^{230}Th dates).

585 Table.1

^{230}Th dating results with the 2σ analytical error.

ML.1

Sample Number	^{238}U (ppb)		^{232}Th (ppt)		d^{234}U* (measured)		^{230}Th / ^{238}U (activity)		^{230}Th Age (yr) (corrected)		d^{234}U$_{Initial}$** (corrected)		^{230}Th Age (yr BP)*** (corrected)	
ML.1.1F	6106	±6	164	±7	-274.2	±0.9	0.0251	±0.0001	3841	±14	-277	±1	3779	±14
ML.1.2F	6222	±6	123	±5	-272.3	±0.9	0.0256	±0.0001	3917	±13	-275	±1	3855	±13
ML.1.3F	6981	±9	72	±4	-271.8	±1.0	0.0257	±0.0001	3923	±12	-275	±1	3861	±12
ML.1.4F	6378	±7	170	±6	-270.3	±0.9	0.0258	±0.0001	3938	±14	-273	±1	3876	±14
ML.1.5F	6674	±8	111	±4	-271.5	±0.9	0.0259	±0.0001	3948	±11	-275	±1	3886	±11
ML.1.6F	7702	±10	189	±5	-270.1	±1.0	0.0260	±0.0001	3964	±11	-273	±1	3902	±11
ML.1.7F	6455	±7	90	±6	-270.7	±0.9	0.0260	±0.0001	3968	±14	-274	±1	3906	±14
ML.1.8F	6144	±7	153	±5	-270.3	±1.0	0.0261	±0.0001	3978	±13	-273	±1	3916	±13
ML.1.9F	6363	±7	122	±6	-270.0	±1.0	0.0262	±0.0001	3989	±15	-273	±1	3927	±15
ML.1.10F	6825	±9	778	±16	-271.5	±1.0	0.0264	±0.0001	4031	±12	-275	±1	3969	±12
ML.1-9a	6395	±6	154	±5	-268.7	±0.9	0.0267	±0.0001	4069	±13	-272	±1	4007	±13
ML.1-10a	7574	±8	132	±4	-267.8	±0.9	0.0272	±0.0001	4138	±12	-271	±1	4076	±12
ML.1-11a	6744	±6	52	±3	-266.2	±0.8	0.0279	±0.0001	4240	±11	-269	±1	4178	±11
ML.1-12a	7716	±8	73	±3	-265.1	±0.9	0.0286	±0.0001	4336	±11	-268	±1	4274	±11
ML.1-13a	7881	±9	127	±4	-262.9	±1.1	0.0290	±0.0001	4386	±13	-266	±1	4324	±13
ML.1-14a	6452	±9	77	±2	-263.8	±1.1	0.0294	±0.0001	4451	±14	-267	±1	4389	±14
ML.1-15a	7392	±10	108	±3	-263.4	±1.0	0.0294	±0.0001	4456	±11	-267	±1	4394	±11
ML.1-16a	6970	±9	441	9	-263.5	1.0	0.0297	±0.0001	4499	±12	-267	±1	4437	±12

ML.2

Sample Number	^{238}U (ppb)		^{232}Th (ppt)		d^{234}U* (measured)		^{230}Th / ^{238}U (activity)		^{230}Th Age (yr) (corrected)		d^{234}U$_{Initial}$** (corrected)		^{230}Th Age (yr BP)*** (corrected)	
ML.2-7	6633	±9	52	±3	-277.0	±1.1	0.0231	±0.0001	3541	±16	-280	±1	3479	±16
ML.2-8	6173	±7	78	±3	-272.6	±1.0	0.0254	±0.0001	3891	±13	-276	±1	3829	±13
ML.2-9	7121	±8	134	±4	-266.0	±1.0	0.0282	±0.0001	4276	±13	-269	±1	4214	±13
ML.2-10	6085	±6	2953	±59	-262.1	±1.0	0.0299	±0.0001	4500	±21	-265	±1	4438	±21
ML.2-9a	6278	±6	106	±4	-257.5	±1.0	0.0306	±0.0001	4603	±17	-261	±1	4541	±17

* δ ^{234}U = ([^{234}U/^{238}U]$_{activity}$ − 1)x1000. ** δ ^{234}U$_{initial}$ was calculated based on ^{230}Th age (T), i.e., δ ^{234}U$_{initial}$ = δ ^{234}U$_{measured}$ x e^{l234xT}.

Corrected ^{230}Th ages assume the initial ^{230}Th/^{232}Th atomic ratio of 4.4 ±2.2 x10^{-6}. Those are the values for a material at secular equilibrium, with the bulk earth ^{232}Th/^{238}U value of 3.8. The errors are arbitrarily assumed to be 50%.

***B.P. stands for "Before Present" where the "Present" is defined as the year 1950 A.D.